ELSEVIER

PII: S0266-3538(97)00111-5

Composites Science and Technology **58** (1998) 91–104

Printed in Northern Ireland
0266-3538/98 $19.00

IMPACT RESPONSE OF WOVEN GLASS-FABRIC COMPOSITES—I. EFFECT OF FIBRE SURFACE TREATMENT

Yasunobu Hirai,[a] Hiroyuki Hamada[a] & Jang-Kyo Kim[b]*

[a]*Department of Polymer Science and Engineering, Faculty of Textile Science, Kyoto Institute of Technology, Kyoto, Japan*
[b]*Department of Mechanical Engineering, Hong Kong University of Science and Technology, Clear Water Bay, Hong Kong*

(Received 5 July 1996; revised 30 May 1997; accepted 25 June 1997)

Abstract

Instrumented impact tests have been employed to study the impact response of vinyl-ester-matrix composites reinforced with woven E-glass fabric. Special emphasis has been placed on an evaluation of the extent of damage and the residual mechanical properties as affected by five different fibre surface treatments. Substantial differences are noted in the shape, mode and area of damage between the front and back surfaces of impact and between the laminates with different fibre surface treatments. Compression-after-impact (CAI) tests were performed to measure the residual compressive strength. A simple model is adopted to predict the threshold impact energy and the threshold damage below which no degradation in residual compressive strength occurs. The major conclusion of the work is that an increase in the γ-MPS silane concentration improves the damage resistance and damage tolerance of the laminates in terms of incipient energy, threshold energy and threshold damage width.

Keywords: A. polymer-matrix composites (PMC), B. fibre/matrix bond, B. impact behaviour, C. damage tolerance, silane coupling agents

1 INTRODUCTION

Damage resistance and damage tolerance under impact loading are the most important characteristics of fibre-reinforced composites because they are vulnerable to accidental impact loading of various kinds during the manufacturing process and in service. Depending on the characteristics of the composite constituents, the choice of fibre and matrix types, laminate configuration and loading geometry, the damage process can be a very complex combination of energy-absorption mechanisms, such as matrix cracking due to transverse shear, transverse fibre fracture and delamination.[1] In particular, the fibre/matrix interphase properties, which are affected by fibre surface treatment, play an important role in determining the failure mechanisms, the extent of damage and the threshold energy of the composite.[2,3] Often this damage may not be visible from the laminate surface, but the presence of this damage substantially reduces the mechanical properties of the composite, especially the in-plane stiffness and strength.[4,5]

Composite laminates containing woven glass fabrics and vinyl ester resins have been devised for applications in the electronics industries, such as printed circuit boards for low-end to mid-range systems, marine vehicle constructions and chemical plants. Fibre composites perform well only when stress can transfer efficiently across the interphase between the fibres and matrix. For this purpose, glass fibres are commonly treated with silane coupling agents. Several factors influence the structure of coupling agent layers and the resultant physical and mechanical properties of the composite made therewith. These are the silane structure in the treating solution and its organofunctionality, drying conditions, the morphology of the fibre and the chemical composition of the surface.[6] In particular, the concentration of silane coupling agent is a critical factor in determining the mechanical performance and fracture behaviour of the composite.[7,8] An established view is that the chemical bonding theory and the interdiffusion theory successfully explain most phenomena observed in silane-treated glass-fibre composites.[6] The interpenetrating network formed at the interphase region as a result of these two adhesion mechanisms consists of chemisorbed and physisorbed layers. An interphase with strong adhesion between the fibre and matrix is expected to give a composite with good shear, compressive and off-axis strengths, and the silane agents applied on the glass fibres make the composites more durable in a hygrothermal environment.[9]

To select the optimum interfacial conditions that would provide balanced mechanical properties, a series of mechanical tests have been performed,[10–12] including tensile, flexural and interlaminar fracture tests. Five different combinations of silane coupling agents were studied: 0·01, 0·4 and 1·0 wt% γ-MPS, methanol-

*To whom correspondence should be addressed.

washed 0·4 wt% γ-MPS and 0·4 wt% γ-GPS (see Section 2.1 for details). The average strength and modulus values obtained from the round-robin test programme[12] are given in Table 1. It is shown that the composites with the lowest γ-MPS concentration (i.e. 0·01 wt%) had the lowest strength both in tension and bending, and an increase in γ-MPS concentration always resulted in the improvement of these properties. A methanol wash of 0·4 wt% γ-MPS marginally increased the modulus and strength. For the composites with 0·4 wt% γ-GPS treatments, the results were very inconsistent between the institutions participating in the round-robin test programme. It was also noted that the modulus averaged for those with five surface treatments was consistently higher in tension than in bending, and the reverse was true for the average strength.[12] In mode I interlaminar fracture tests,[10,11] surface treatments with 0·01 wt% γ-MPS and 0·4 wt% γ-GPS agents showed quite stable crack growth with plateau fracture toughness values consistently higher than for the other silane agent treatments. In contrast, intermittent stable and unstable crack propagation was observed for the laminates containing 0·4 and 1·0 wt% γ-MPS coupling agents, with correspondingly low fracture toughness values.

In the present study, a continuation of the previous papers,[10–12] damage resistance and damage tolerance of composites under impact loading are evaluated. Fundamental understanding of the impact response of glass-fibre composites is considered essential to proper evaluation of the silane coupling agents. The damage modes and shapes are characterised qualitatively, and the damage areas are measured quantitatively. Of special interest is the correlation between the extent of damage and residual strengths for different fibre surface treatments. The threshold impact energy and threshold damage area are also evaluated on the basis of a simple exponential model.

2 EXPERIMENTAL PROCEDURES

2.1 Materials and fabrication of composite laminates

The fibres, matrix material, silane coupling agents and fabrication procedures of the composite laminates employed in the present study were basically the same as those reported previously.[12] The E-glass (WE18W) fibres were supplied by Nitto Boseki Co., Japan, in the the form of a plain-woven fabric which contained 44 (warp)×34 (weft) strands per 2·5 cm×2·5 cm area. Each strand consisted of 400 filaments of 9 μm in diameter. The matrix material was made from an unsaturated vinyl ester resin (Ripoxy R806), supplied by Showa High Polymer, Japan, which was polymerised with 0·7 wt% methyl ethyl ketone peroxide. Two different coupling agents were used: A-174 γ-methacryloxypropyltrimethoxysilane (γ-MPS) and A-187 γ-glycidoxypropyltrimethoxysilane (γ-GPS), supplied by Nippon Unicar Co., Japan. The γ-MPS has an organic function that can react with the double bond of the vinyl ester resin, while γ-GPS has no such double bond in its molecular structure.[7] The aqueous solutions of silane coupling agents were acidified with acetic acid at pH 4·0. Five different combinations of silane coupling agents were used for fibre surface treatment: 0·01, 0·4 and 1·0 wt% γ-MPS, methanol-washed 0·4 wt% γ-MPS, and 0·4 wt% γ-GPS. The glass fabrics were dipped into the aqueous solutions of the silane agents, and then subsequently squeezed between rollers and dried for 10 min at 110°C.

Twenty-ply laminates were prepared by hand lay-up with all warp strands being placed in the same direction. The laminates were cured for 48 h at room temperature, followed by post-cure for 3 h at 80°C and for 2 h at 150°C in an oven. The average fibre volume fraction was approximately 0·426,[12] and the nominal thickness of the plate was 4 mm.

2.2 Specimens and tests

Impact tests were conducted on 100 mm×100 mm square laminate specimens at room temperature on a Ramana ITR-2000 instrumented impact tester.[13,14] Fig. 1 shows schematically the general arrangement of the instrumented impact tester. The impactor consisted of a hemispherical nose of 12·7 mm in diameter and a loading rod of 200 mm in total length including the nose. The specimen centre was impacted while its edge was firmly fixed between two circular rings having a test window of 75 mm in diameter. The incident energy was varied by changing the height of the impact nose relative to the specimen so that the displacement of the impactor could be controlled. In the present study, the

Table 1. Strengths and moduli of woven glass-fabric-reinforced vinyl-ester-matrix composites measured in the weft direction.[12] (Mean values ± standard deviation)

Type and concentration of silane agent (wt%)		Strength (MPa)		Modulus (GPa)	
		Tension	Bending	Tension	Bending
γ-MPS	0·01	270 ± 21	372 ± 20	19·5 ± 5·2	18·1 ± 1·5
	0·4	318 ± 16	431 ± 19	19·6 ± 5·1	18·8 ± 1·6
	1·0	329 ± 31	444 ± 40	20·2 ± 5·2	19·7 ± 1·9
Methanol-washed γ-MPS	0·4	338 ± 13	452 ± 23	20·4 ± 5·0	19·4 ± 0·9
γ-GPS	0·4	321 ± 32	380 ± 27	20·3 ± 5·0	19·3 ± 1·1

applied impact energy level was in the range 19–47 J and introduced non-penetrating damage to the laminates with all five different fibre surface treatments. The velocity of the impactor at the moment of first contact with the specimen was almost constant in the range 1·7 to 2·0 m s^{-1}, regardless of the total energy applied or the type of fibre surface treatment. The load/displacement records were obtained directly from the data-acquisition system via the impactor equipped with a piezoelectric device. After the prescribed impact, the specimens were examined microscopically to assess the modes of damage sustained, and the damage areas on the front and back surfaces of the specimen were measured with the aid of an image analyser.

Compression-after-impact (CAI) tests were employed to evaluate the damage tolerance of the composite, which refers to the ability to perform given a specified amount of damage.[15] The residual compressive strengths corresponding to applied impact energy levels and damage areas were measured on a fixture fabricated in accordance with the Boeing Specification Support, Standard BSS 7260, as shown in Fig. 2. The fixture imposed clamped boundary conditions on the load ends and simply-supported boundary conditions on the side edges to prevent out-of-plane buckling of the specimens. Compressive loads were applied in the weft direction of the laminates with an MTS universal testing machine, and all tests were conducted at a crosshead speed of

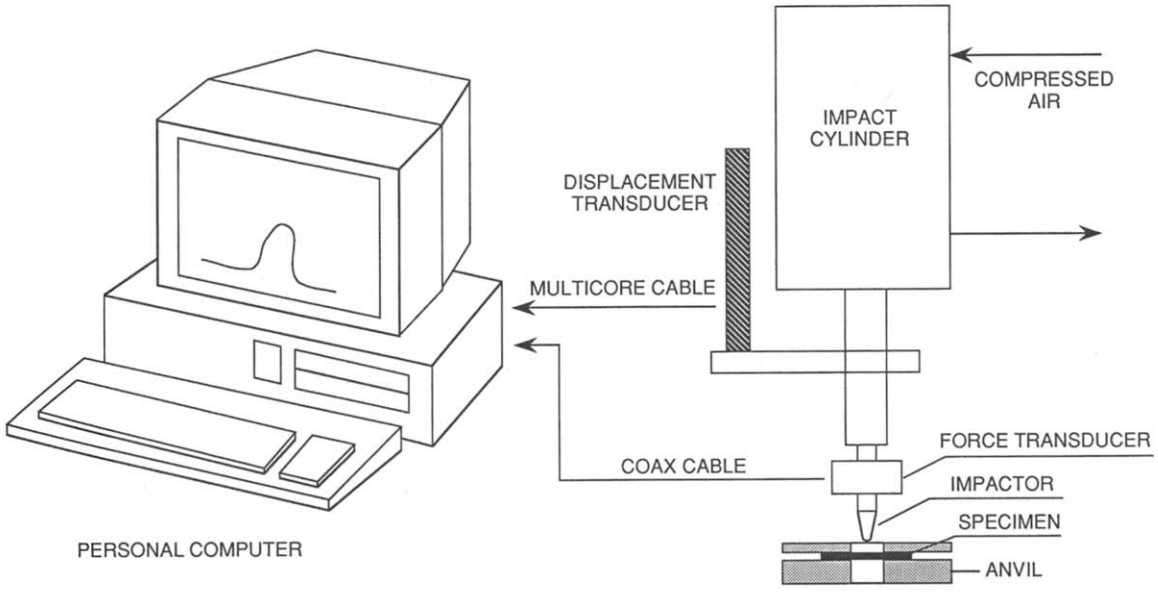

Fig. 1. General arrangement of the Ramada ITR-2000 impact tester.

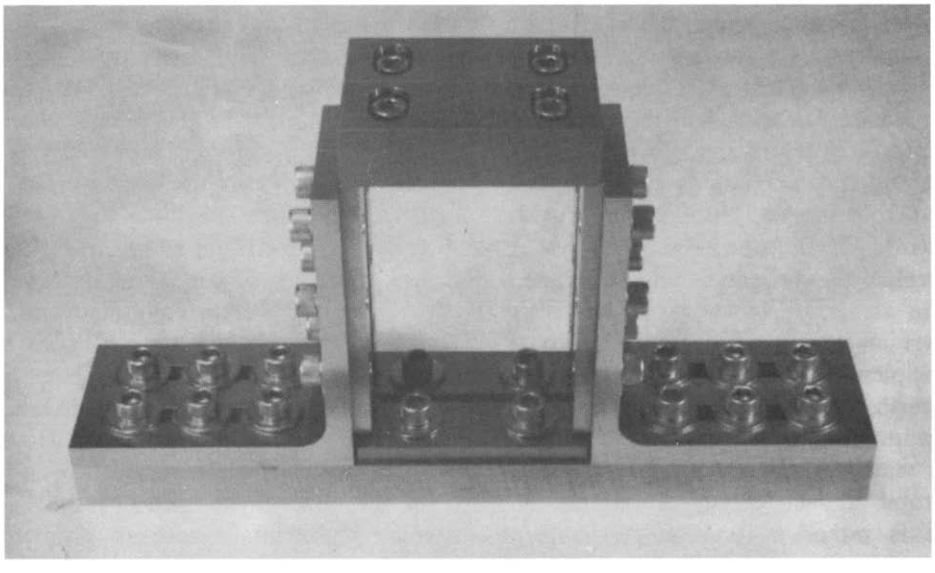

Fig. 2. Compression-after-impact (CAI) test fixture.

0·5 mm min^{-1} at room temperature. The compressive strengths of undamaged specimens were also measured.

3 RESULTS

3.1 Load/displacement curves

Very smooth load/displacement records with little oscillation were obtained with the displacement-controlled impact tester. Otherwise, large oscillation would have occurred as in most drop-weight impact testers owing to the dynamic inertial effect. The load/displacement curves recorded for impact tests varied according to the severity of the impact, with little difference between different fibre surface treatments. Figure 3 depicts typical load/displacement curves for the laminates with different types of silane coupling agent, which look essentially similar. The characteristic load points[16] of these curves include the incipient damage load, P_i, and maximum load, P_m [Fig. 3(a)]. The incipient damage load, or the first failure point,[17] can be identified by the first sudden load drop and/or change in slope in the ascending portion of the load, as a consequence of interface failure or matrix cracking near the back surface of the laminate.[18] Beyond the incipient damage load, the residual strength can be influenced significantly by the impact energy owing to damage growth within the laminate. On the other hand, the maximum load represents the peak load that a laminate can tolerate before undergoing major damage. The failure load, P_f, at which the laminate loses its structural integrity was not clearly identified in the present study. The initial gradient of the ascending straight line can be regarded as a measure of the rigidity of the material. The energies applied to the laminate up to the corresponding load points are the incipient energy, U_i, the energy to peak, U_m, and the post-peak energy, U_p, which can be measured by the respective areas under the load/displacement curve [Fig. 3(a)]. The total impact energy applied to the laminate equals the sum of the energy to peak and the post-peak energy: i.e. $U = U_m + U_p$. The post peak energy is a measure of the energy required for damage propagation.[16]

Figure 4(a),(b) present the relationships between the characteristic impact loads and the impact energies, which are obtained from the load/displacement curves. Each symbol shown in the following figures represents one experimental value. It was found that the incipient damage loads were almost constant regardless of the impact energy level and the type of silane agent. It appears that the incipient damage load was not sensitive enough to distinguish the difference in fibre surface treatment. Damage initiation in the laminate in terms of interface failure or matrix cracking should also be independent of the total impact energy. It seems that damage initiation is rather a function of incipient impact energy, U_i, which is a measure of the ability of the laminate to resist the damage initiation, or to sustain an event without damage (i.e. damage resistance).[15] The incipient energy, U_i, is distinct from the threshold energy, U_0, in that the threshold energy is a measure of the ability to resist initial strength degradation due to impact damage (i.e. damage tolerance). In this respect, damage tolerance is a function of the damage present, rather independent of the method of introduction. It seems that there was minor confusion regarding the exact definitions of these impact energy parameters in previous papers.[17] Damage resistance and damage tolerance are two distinct fracture properties although both characteristics are the direct reflection of the microstructure of the materials concerned.

The maximum load increased almost linearly with increasing impact energy for all fibre surface treatments studied. All data points fell within a narrow spectrum of variation, showing little difference between different surface treatments. It was noted previously[18] that at the maximum load, major fibre breakage occurred through the laminate thickness, starting from the back face towards the front face. The maximum load was normally followed by a predominant load drop which is an indication of the reduction in the laminate rigidity.[16]

3.2 Impact damage modes and damage area

The damage modes were characterised by using an optical microscope from the front and back surfaces of the laminate with the aid of high-intensity transmitted and reflected light. The C-scan ultrasonic flaw detector was also tried to characterise the damage modes, with little success. At low impact energies, the external appearance for all composites with different fibre surface treatments was similar, consisting of contact-induced plastic indentation or concentrated flexure with only slight crushing to a circular shape at the point of impact.

With increased impact energy, damage became more extensive in the form of matrix cracking, transverse fibre fracture and delamination. Figure 5 shows the damage on the front and back surfaces of the laminates which were impacted with an energy of approximately 30 J at a constant punch height. On the front surface, which had direct contact with the punch, the damage area was represented by a cross shape with the points lying in the warp and weft strand directions. These observations are illustrated schematically in Fig. 6. The major cracks were invariably slightly longer in the weft direction than in the warp direction. These damage features extended to a certain depth through the thickness of the laminate, without changing the overall shape.

The damage modes on the back surface were more diverse and complicated. To illustrate clearly the various damage modes, a schematic drawing is presented in Fig. 7, and a magnified photograph is shown in Fig. 8 for the upper right-hand corner of the whole damage area. The damage area is divided into four major regions[19] which represent different damage modes: region A with major damage including extensive

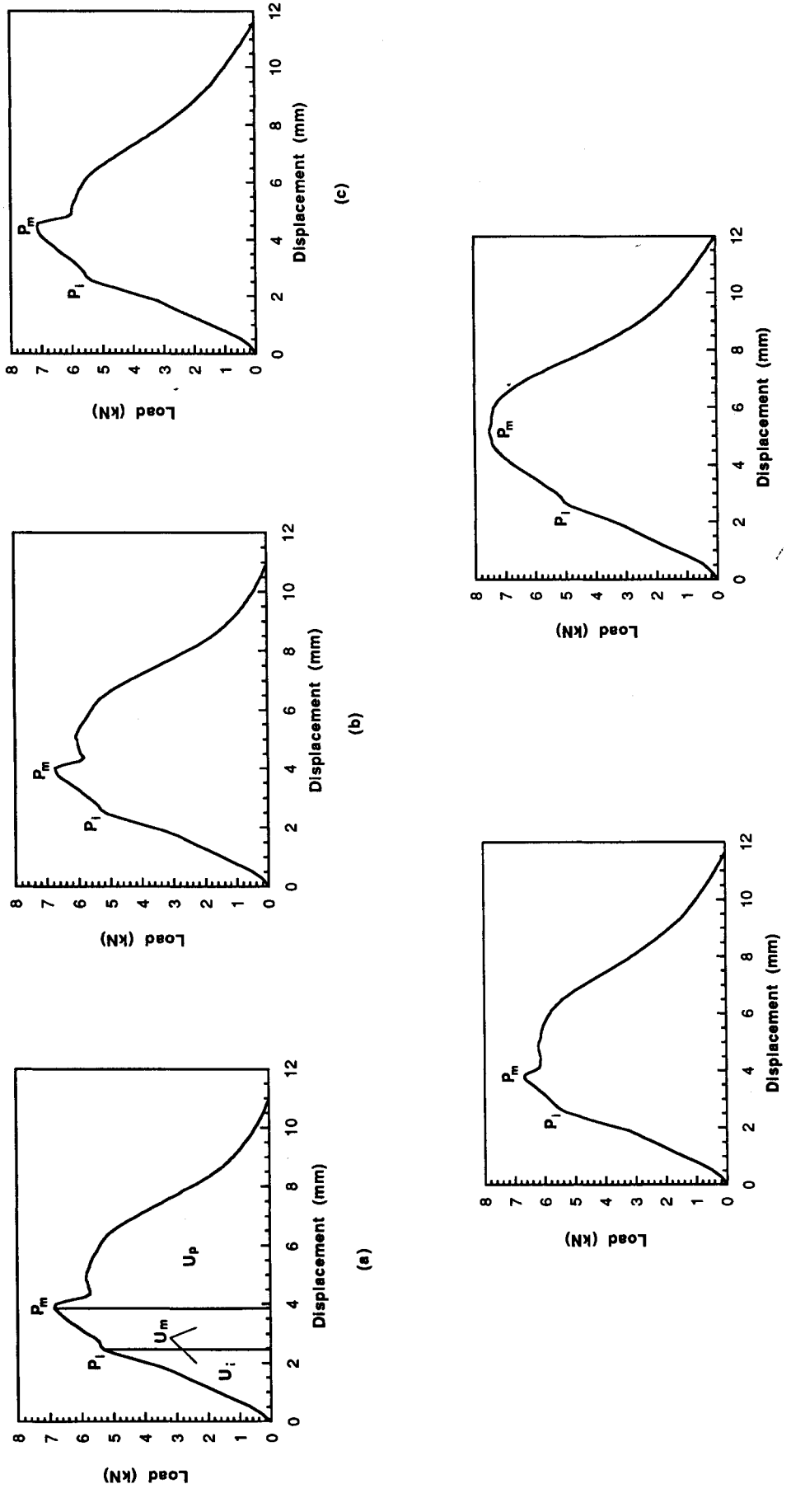

Fig. 3. Typical load/displacement curves obtained from the instrumented impact test: (a) 0·01 wt% γ-MPS; (b) 0·4 wt% γ-MPS; (c) 1·0 wt% γ-MPS; (d) methanol-washed 0·4 wt% γ-MPS; (e) 0·4 wt% γ-GPS.

delamination, matrix cracking and transverse fibre fracture; region B with fibre/matrix interface debond cracks both in the warp and weft directions; region C with interface debond cracks in the warp direction; and region D with interface debond cracks in the weft direction.

The major damage that occurred in the central damage region (region A) had a four-point star shape which was slightly elongated in the warp direction. With reference to Figs 6 and 7, quantitative comparisons are made between the damage lengths in the warp and weft directions which are measured from the central regions of the front and back faces of the laminates, as shown in Fig. 9. It is interesting to note that on the front face the major cracks are longer in the weft direction than in the warp direction, while the reverse is true for the major cracks on the back surface. These damage modes have a significant implication on the failure mechanisms and the residual strength to be measured in the subsequent compression tests.

Close examination of the localised debonding surrounding the major damage area in Figs 7 and 8 revealed that the damage area due to interface debonding was longer in the warp direction than in the weft direction. This result appears to be a reflection of the woven fabric configuration used in the present study, such that the warp strands have a larger surface area

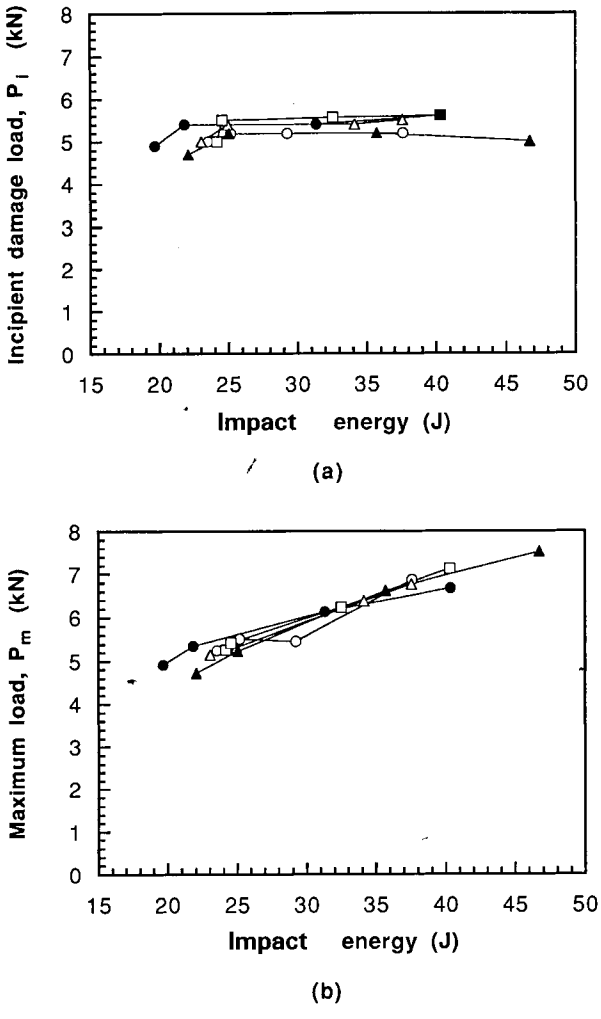

Fig. 4. Plots of (a) incipient damage load, P_i, and (b) maximum load, P_m, as a function of impact energy: ○, 0·01 wt% γ-MPS; △, 0·4 wt% γ-MPS; □, 1·0 wt% γ-MPS; ●, methanol-washed 0·4 wt% γ-MPS; ▲, 0·4 wt% γ-GPS.

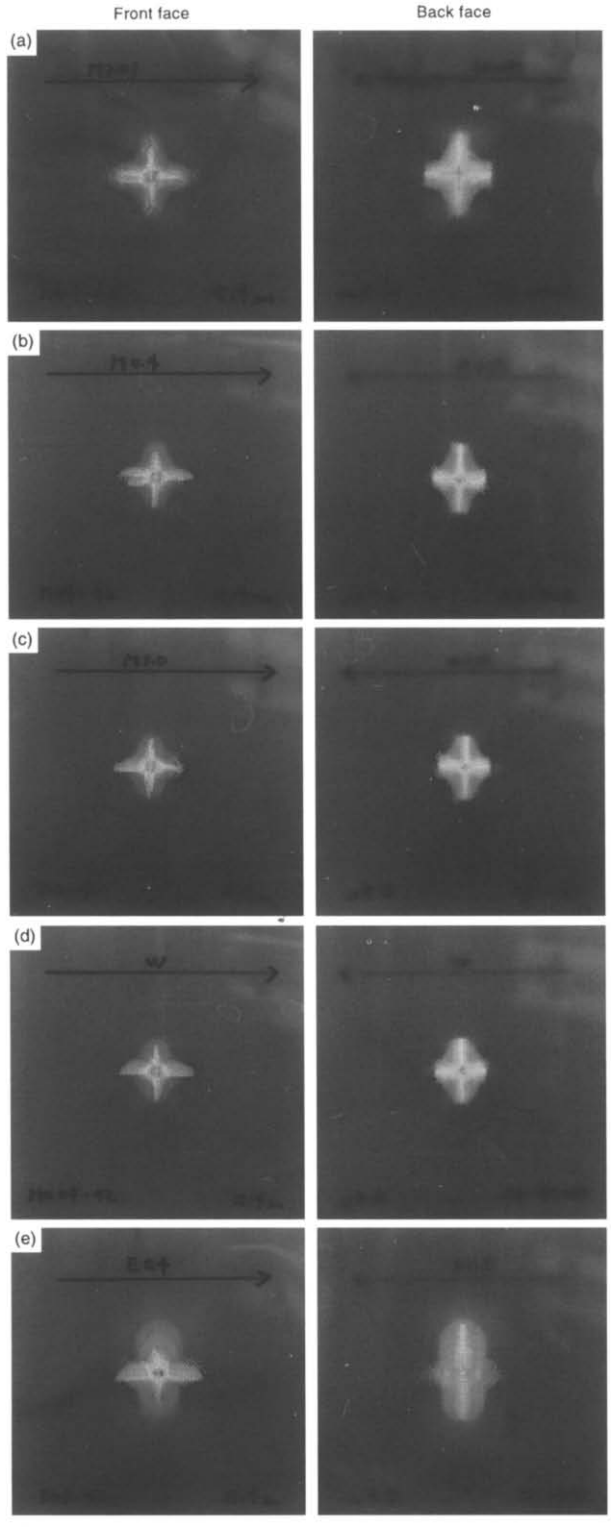

Fig. 5. Photographs of the front and back surfaces of typical damaged laminates: (a) 0·01 wt% γ-MPS; (b) 0·4 wt% γ-MPS; (c) 1·0 wt% γ-MPS; (d) methanol-washed 0·4 wt% γ-MPS; (e) 0·4 wt% γ-GPS.

than the weft strands. Therefore, the total damage area (i.e. the sum of regions A, B, C and D) had an oval shape resembling the shape of the central damage region A. It is also noted that the interface debond cracks in regions B, C and D appeared only in the last two or three plies adjacent to the back surface, and they could not be detected from the front surface. These debond cracks were detected from the back faces of all specimens tested in the present study, and remained mostly inside the laminate without extending to the back surface, except for a few isolated examples. This observation suggests that the interface debond cracks propagated in the early stage of the damage process, probably at or after the incipient impact force [Fig. 3(a)], before the major cracks had propagated in the central region. It was argued that the major fibre breakage commenced from the back face, followed by penetration into the front face.[18] The laminates whose fibres were

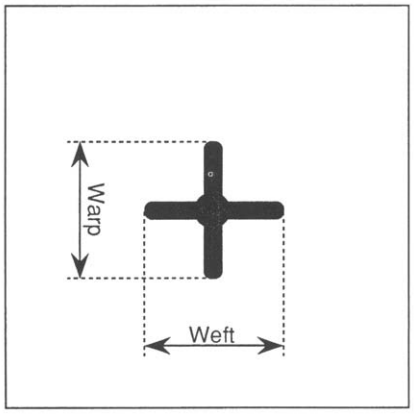

Fig. 6. Schematic illustration of major damage on the front surface of the laminate.

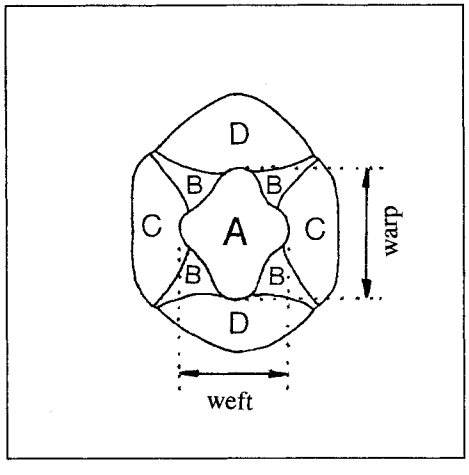

Fig. 7. Schematic illustration of typical damage on the back face of the laminate subjected to an impact energy of 30 J. Regions A, B, C and D represent different damage modes: A = extensive damage due to delamination and fibre breakage; B = interface debonding both in the warp and weft directions; C = interface debonding in the weft direction only; and D = interface debonding in the warp direction only.

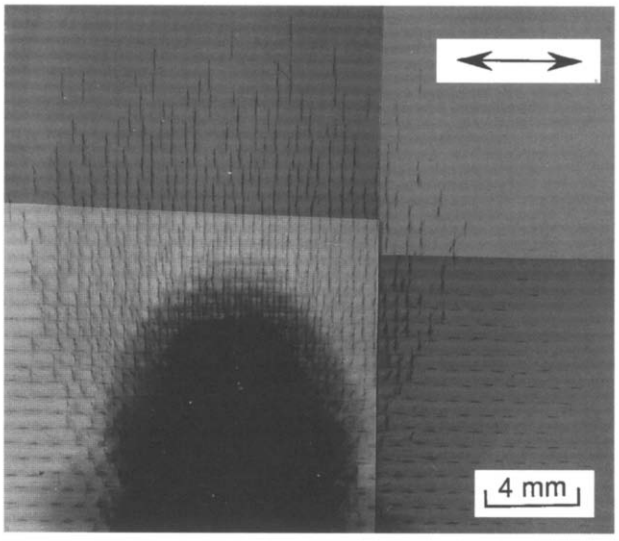

Fig. 8. A magnified view of the interface debonding at the upper right-hand corner of the damage area in Fig. 7. The arrow indicates the weft direction.

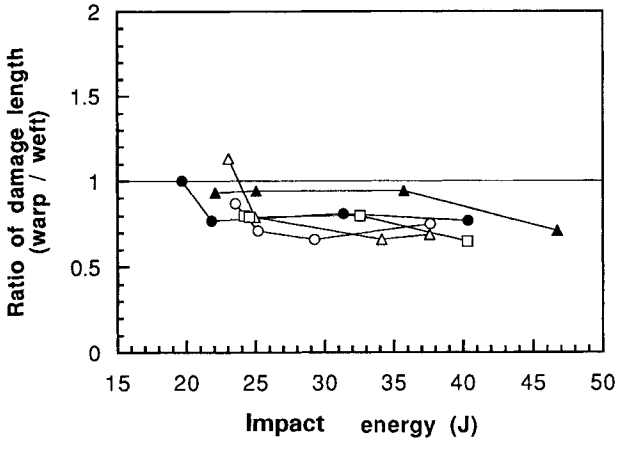

(a)

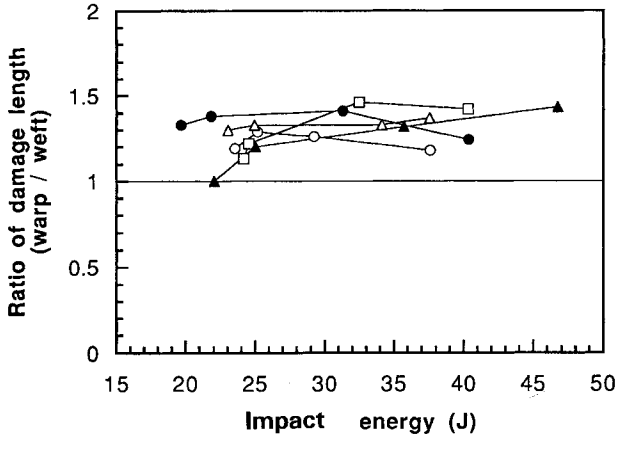

(b)

Fig. 9. Ratio of damage length in the warp direction to that in the weft direction: (a) on the front face; (b) on the back face. Symbols as in Fig. 4.

treated with different silane agents showed basically similar features as described above, except for the total damage area.

The damage area plotted as a function of the impact energy in Fig. 10 clearly indicates that the back surface of the laminate suffered much more damage than the front surface. This is a typical impact damage mode for most angle-ply laminate composites, having a conical shape in the thickness direction with the overall in-plane damage area increasing from the direct impact surface to the back surface.[1] The central major damage area increased gradually with increasing impact energy both on the front and back surfaces [Fig. 10(a),(b)], with little variation between the laminates having different prior fibre surface treatments. The central delaminated area accounted for approximately 10–25% of the total damage area on the back surface, depending on the impact energy.

The total damage area measured on the back surface showed large variation between the different surface treatments [Fig. 10(c)], although the general trends of increasing damage area with increasing impact energy were essentially similar. It is worth noting that the laminates with 0·4 wt% γ-GPS and 0·01 wt% γ-MPS treated fabrics had much larger damage areas than the other laminates. This observation appears to be consistent with the slightly lower incipient damage loads obtained for the laminates with the above silane treatments, as shown in Fig. 4(a). As the interface debonding accounted for the majority of the total damage area, a large total damage area seems to be directly related to brittle nature of the fibre/matrix interphase properties affected by the type and concentration of coupling agent. Although the presence of such interface debond cracks did not reduce substantially the static residual compressive properties, to be discussed in the next section, they would have detrimental effects on the long-term mechanical properties of the laminates, especially in temperature cycles and under humid environment. Such interface cracks may act as nucleation sites for permeated moisture, and tend to coalesce to form main cracks.

3.3 Residual strength, threshold energy and threshold damage

3.3.1 Analytical model

Experiments on carbon- and glass-fibre composites[5,17,20–22] have shown that there exists an impact energy threshold below which strength reduction does not occur. A simple model of residual strength[23] has been developed to correlate the residual strength after impact, σ_r, to the threshold impact energy, U_0, and the threshold damage, c_0:

$$\frac{\sigma_r}{\sigma_0} = \left(\frac{c_0}{c}\right)^{\alpha} = \left(\frac{U_0}{U}\right)^{\beta} \quad (1)$$

where σ_0 is the original strength not affected by cracks smaller than the threshold value, c_0. c is the notch length or equivalent damage area (or, more appropriately, damage width). U_0 represents the threshold impact energy that the material can withstand without any strength degradation. The threshold values, c_0 and U_0,

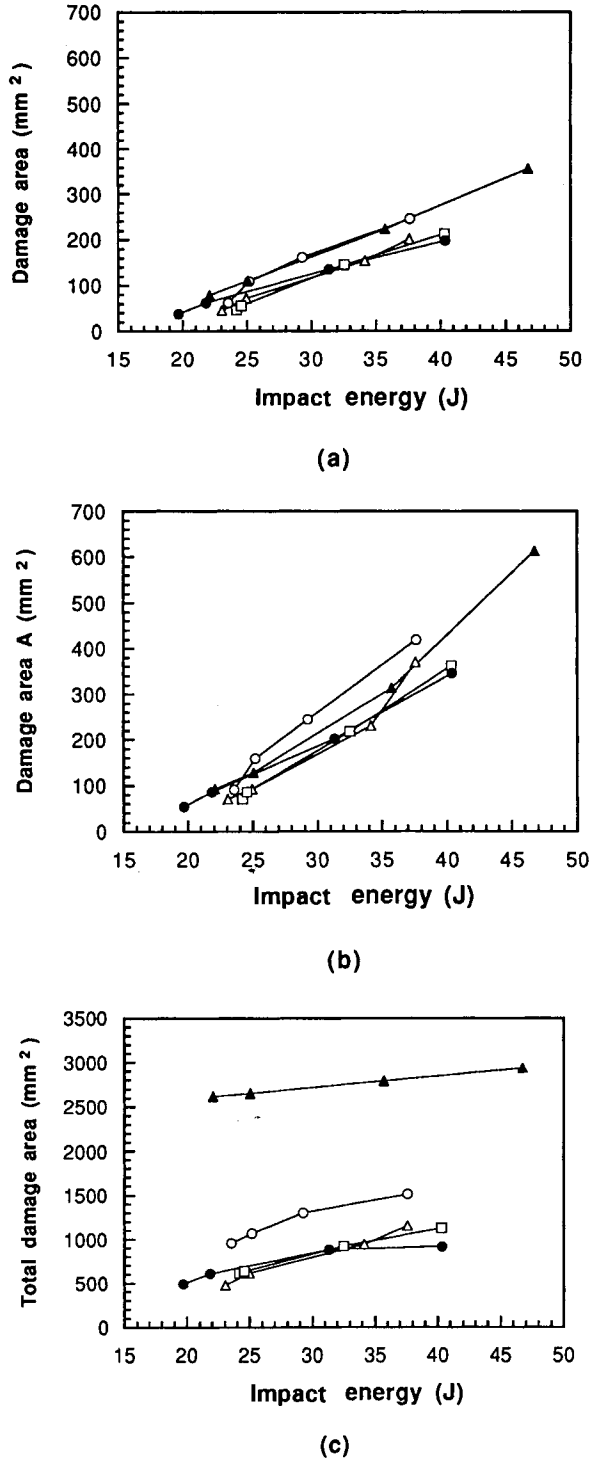

Fig. 10. Damage areas versus impact energy: (a) on the front face (Fig. 6); (b) central damage area (region A of Fig. 7) on the back face; (c) total damage area on the back face (regions A, B, C and D in Fig. 7). Symbols as in Fig. 4.

and the exponents, α and β, can be determined from the least-squares fitted log–log plots of residual strength data:

$$\log \sigma_r = \log \sigma_0 + \beta(\log U_0 - \log U)$$
$$\log \sigma_r = \log \sigma_0 + \alpha(\log c_0 - \log c) \quad (2)$$

Behind the relationships given by eqn (1) is a simple power-law assumption[17] for the impact energy and the equivalent notch dimension:

$$c = kU^n \quad (3)$$

which is valid only when the damage size is greater than the threshold value: $c \geq c_0$. However, there are situations where the laminates deform only elastically upon impact without causing any appreciable damage if the applied energy is lower than a certain critical value. It is therefore necessary to modify eqn (3) to accommodate the idea of the incipient energy, U_i, which represents the minimum energy required to introduce damage in the laminate:

$$c = k(U - U_i)^n \quad (4)$$

which is valid for $c \leq c_0$. The incipient energy, U_i, can be determined experimentally from the impact force/displacement curves [see Fig. 3(a)], as suggested previously.

3.3.2 Residual compressive strength

The increase in damage area for all materials with increasing impact energy is matched by a reduction in compressive strength with impact energy. The residual compressive strengths of damaged specimens normalised with those for undamaged specimens, σ_r/σ_0, are plotted in Figs 11 and 12(a),(b) as a function of impact energy, damage width and damage area, respectively. A larger major damage length and a larger major damage area determined from the central damage region of the front and back faces of the laminate were regarded as the damage width and the damage area, respectively, in Fig. 12(a),(b). Damage width, instead of damage area, was used here to calculate the damage parameters, α and c_0, with eqns (1) and (2), and thus to evaluate the correlation with the residual compressive strength. This approach has been justified by the fact that the impact damage grows laterally transverse to the loading direction in the CAI test, which showed a prominent dependence of the residual properties on damage width.[24–26] Otherwise, the damage area A in Fig. 7 was used as the damage parameter for the analysis of incipient energy, U_i, in eqn (4).

The threshold values, U_0 and c_0, and the damage exponents, α and β, were obtained from the linear-squares fitting analysis of eqn (2), and are presented in Table 2. The analytical predictions for the laminates with five different surface treatments are superimposed in the corresponding Figs 11 and 12. Also included in Fig. 12(a) is a diagonal line representing the strength

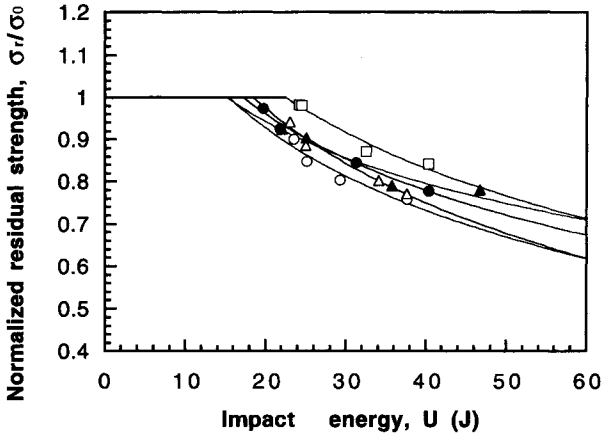

Fig. 11. Normalised residual compressive strength, σ_r/σ_0, versus impact energy, U. Symbols as in Fig. 4, and solid lines represent the analytical predictions.

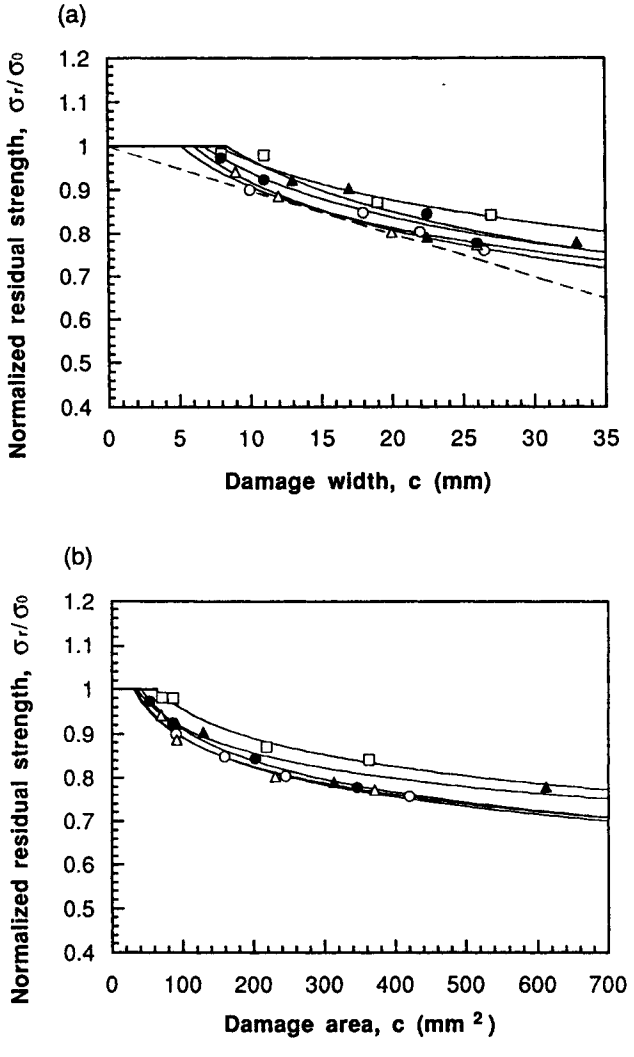

Fig. 12. Normalised residual compressive strength, σ_r/σ_0, plotted as a function of (a) damage width and (b) damage area. Symbols as in Fig. 4. The dashed line in (a) represents the prediction calculated on the basis of a reduction in cross-sectional area.

Table 2. Threshold energy, U_0, threshold damage width, c_0, and corresponding exponents, α and β

Type and concentration of silane agent (wt%)		Impact energy		Damage width	
		U_0 (J)	β	c_0 (mm)	α
γ-MPS	0·01	16·3	0·34	5·72	0·17
	0·4	19·0	0·38	6·42	0·19
	1·0	22·6	0·32	7·90	0·14
Methanol-washed γ-MPS	0·4	17·5	0·30	6·99	0·17
γ-GPS	0·4	15·9	0·25	8·92	0·20

degradation which would be expected as a consequence of the decrease in effective cross-sectional area of the specimen, without considering the notch sensitivity of the specimen.[26]

The plots presented in Figs 11 and 12(a),(b) confirm the general trends, showing that the residual strength falls parabolically with increasing impact energy and the corresponding damage width. Although small groups of specimens were tested for each set of conditions, there is a clear indication of a correlation with little data scattering between the residual compressive strength and impact energy as well as between the residual compressive strength and damage width. It is noted that the residual strength predicted on the basis of the effective cross-sectional area was slightly lower than the experimental values [Fig. 12(a)], indicative of insensitivity of the materials to the presence of sharp cracks. The partial damage through the specimen thickness is responsible for the higher experimental residual strengths than the prediction.

The distinction between some of the five silane agents is quite consistent in terms of the impact parameters, suggesting that their relative performance in damage tolerance can be clearly identifiable. It is noted that the increase in γ-MPS silane concentration improved the threshold impact energy, U_0, and the threshold damage width, c_0 (Table 2). The trends of strength degradation

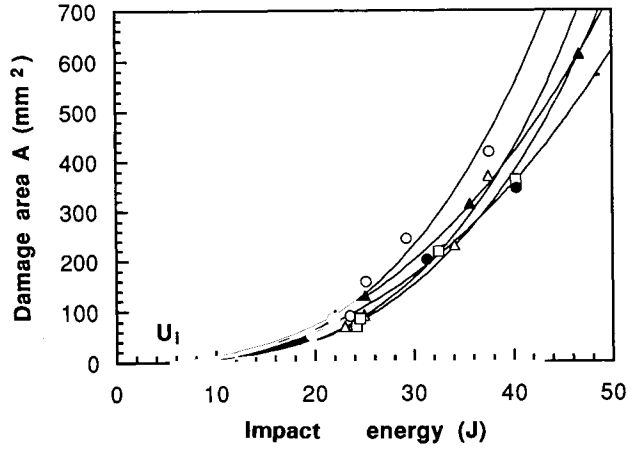

Fig. 13. Re-plots of damage area versus impact energy of Fig. 9(b), showing the incipient impact energy, U_i. Symbols as in Fig. 4. The solid lines represent the analytical predictions.

beyond the threshold values, U_0 and c_0, were quite consistent [Figs 12(a),(b) and Table 2]. The laminates containing γ-GPS and methanol-washed 0·4 wt% γ-MPS treated fabrics performed intermediate in terms of strength degradation. It should be mentioned here that all data points included in these figures are for the laminate specimens which failed consistently across the central region.

3.3.3 Incipient impact energy

Figure 13 is redrawn with the experimental data taken from Fig. 10(b) to determine the incipient impact energy, U_i, using the linear-squares fitting of log–log plots of eqn (4). The analytical predictions are superimposed in Fig. 13, and the incipient energies are obtained from the points where the curves intersect the abscissa. Table 3 compares the analytical predictions with the average values of the experimental measurements obtained from the load/displacement curves [Fig. 3(a)]. It is worth noting that the experimental measurements agree reasonably well with the analytical results for all surface treatments, except for a couple of isolated data points whose result may have been associated with the limited number of specimens tested. In general, an increase in silane concentration of γ-MPS slightly enhanced the incipient energy, and methanol wash of γ-MPS treated fibres reduced the incipient energy. The lowest incipient energies were obtained for the laminates made with γ-GPS treated glass fabrics, both from the experiments and the analysis. All these observations are considered to be consistent with the above results on threshold impact energy and threshold damage width. It is recalled that the incipient energy is

Table 3. Comparison of the incipient impact energy, U_i, measured from the impact load/displacement curves and the analytical prediction based on eqn (3)

Type and concentration of silane agent (wt%)		U_i (J)	
		Experiments	Analysis
γ-MPS	0·01	5·90	4·89
	0·4	6·80	6·28
	1·0	6·85	6·03
Methanol-washed γ-MPS	0·4	6·41	3·84
γ-GPS	0·4	6·01	3·65

the minimum impact energy required to introduce damage in the laminate, whether the induced damage is sufficient to cause strength degradation or not.

3.4 Failure mechanisms in CAI tests

Typical failure mechanisms that took place on the front and back faces of the laminates in compression-after-impact tests are shown schematically in Fig. 14. Microphotographs taken from the cross-section of the central damage region (see the inset) for specimens showing the corresponding failure mechanisms in Fig. 14 are presented in Fig. 15. Three major failure mechanisms were identified: failure has been initiated (i) by the damage present near the front surface [Fig. 14(a)]; (ii) by the combination of the damage near the front and back surfaces [Fig. 14(b)] and (iii) by the damage present near the back surface [Fig. 14(c)]. The cross-sectional view of the failure mode (i) in Fig. 15(a) clearly indicates that, during compression, the main crack initiated from the existing damage in the front face and propagated obliquely across the laminate thickness towards the back face, bypassing the major damage present near the back surface. In contrast, other specimens shown in Fig. 15(b),(c) failed apparently by the cracks propagating from the existing damage on the back face, and the damage present near the front face contributed to a lesser extent to the final failure of the laminate. It appears that extensive delamination occurred over the whole central region before instability due to gross collapse by plastic buckling.[27] However, no specific failure mechanisms were identified which corresponded to different silane treatments, applied impact energy and damage size.

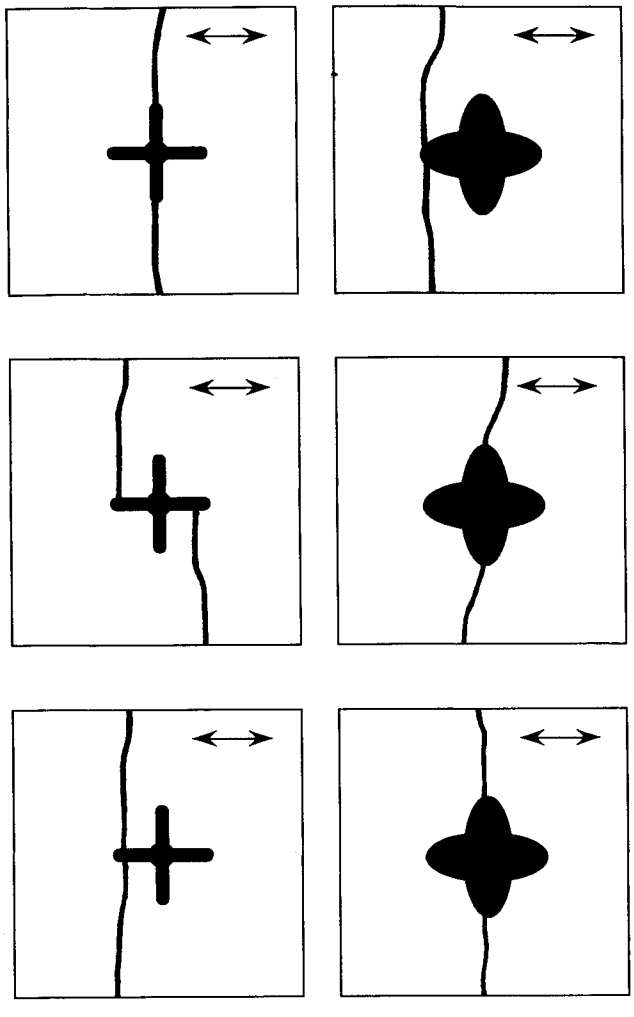

Fig. 14. Schematic representation of typical failure mechanisms on the front and back surfaces of compression-after-impact test specimens. Specimens failed by: (a) cracks present near the front surface; (b) the combination of cracks present near the front and back surfaces; (c) cracks present near the back surface. The arrows indicate the weft direction.

4 DISCUSSION AND CONCLUDING REMARKS

In light of the experimental and analytical study presented in the foregoing sections, the implications can be summarised with regard to the impact damage resistance and impact damage tolerance of the composite laminates with different silane agents and concentrations. It is clear that the incipient damage loads were little affected by the impact energy and the types of fibre surface treatment [Fig. 4(a)]. In contrast, the incipient energy determined from the load/displacement curves and the analysis of the power-law equation increased marginally with silane concentration within the allowable data scattering. The incipient energy is the elastic strain energy stored in the laminate before inelastic deformation occurs owing to damage initiation. In view of the marginal improvement in modulus with the increase in silane concentration (Table 1), it appears that the difference in the incipient energy simply reflects the slight difference in modulus effected by the different interphase conditions surrounding the fibre. This is attributed[10] to the fact that the excess γ-MPS at a high silane concentration diffused into the vinyl ester resin during the curing process to form a physisorbed layer that is stiffer and more brittle than the bulk matrix resin. A similar finding has been reported that improvement in the fibre/matrix interface bond strength resulted in a significant increase in the incipient energy required for damage initiation in a carbon-fibre/epoxy system.[2] Although the strong interface bond resulting from fibre surface treatments also reduced the level of damage for a given input energy, the increased notch sensitivity of the laminate arising from the brittle interphase had a detrimental effect on residual strength in tension.[28]

It is thought that the interface debonding observed on the back face of impact took place at or immediately after the incipient load point. Additional impact tests were performed with the total applied energy being slightly greater than the incipient energy as determined previously (Fig. 13). The maximum load was maintained lower than the incipient damage load given in Fig. 4(a). While there occurred no major damage due to

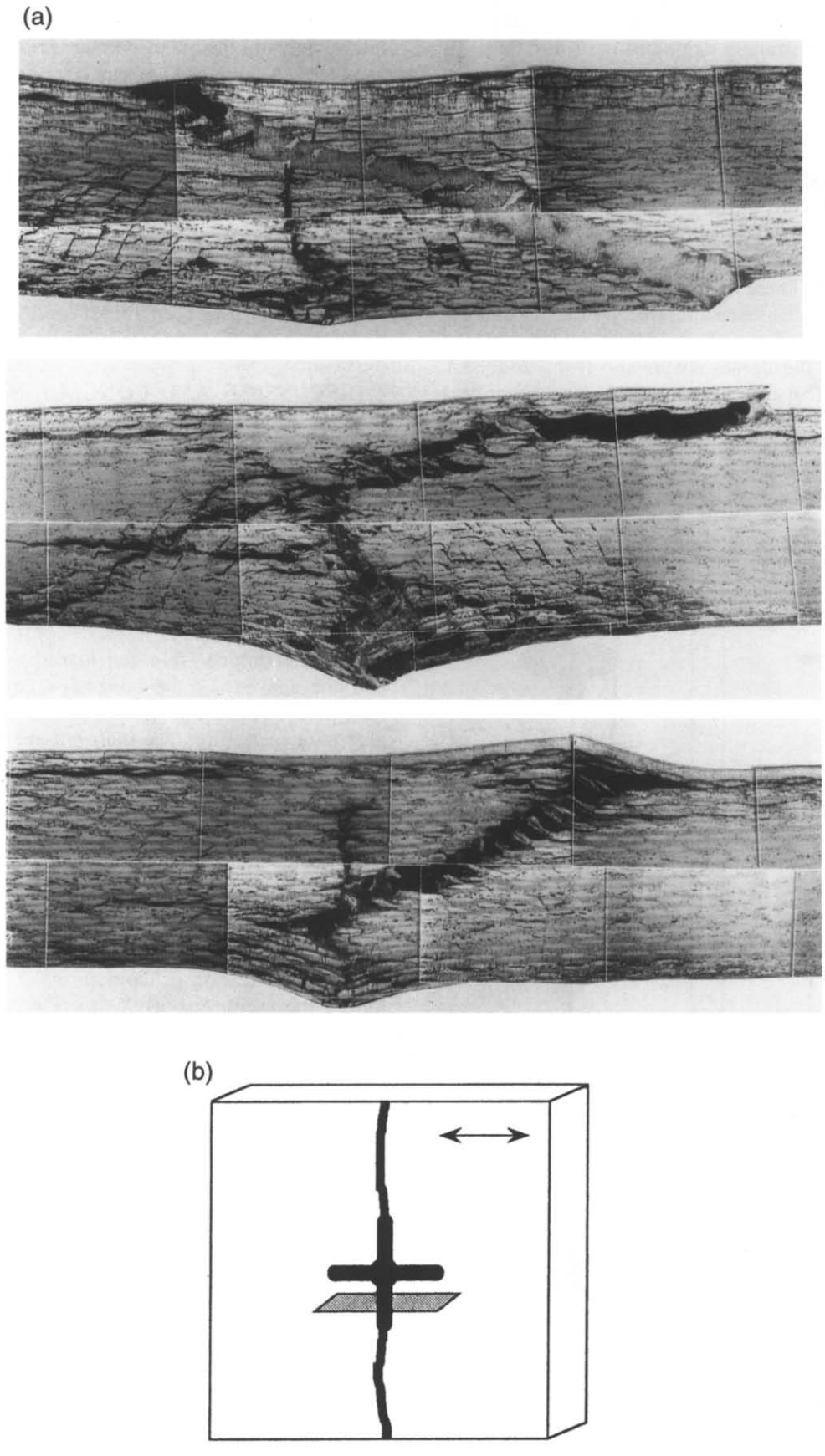

Fig. 15. (a) Microphotographs of the cross-sections at the central damage region of the specimens in (b), which correspond to typical failure mechanisms shown in Fig. 14.

delamination and fibre breakage on either side of the laminate, interface debond cracks appeared on the back face of impact. This partly confirms the above hypothesis that the incipient energy is a measure of the ability of the material to resist initial damage due to interface debonding on the back face of impact. It is also worth mentioning that the differences between the incipient energies, U_i, and the threshold energies, U_0, are found to be quite substantial, approximating 10 J for most surface treatments, as seen by comparing Tables 2 and 3. According to the definitions of these two energy parameters, the extent of damage generated by the impact energy levels is not sufficient to cause any appreciable degradation of the residual strength.

It should be mentioned here that no direct correlation has been established between the total damage area (or total damage width) and the residual compressive strength. This supports the view that the interface debonding, which occurred only in several layers adjacent to the back surface of the laminate, has little effect on strength degradation, although the debond cracks account for approximately 75% of the total debond area. This may also imply that a laminate which displays the best performance in damage resistance (i.e. the highest incipient energy) may not necessarily perform the best in damage tolerance (i.e. the highest threshold energy and threshold damage) as these two damage parameters are measured in different fracture modes. In other words, the damage resistance and the damage tolerance are different fracture properties although both characteristics are the direct manifestation of the microstructural properties of the materials concerned.

Judging from the loading configuration of the impact test, damage resistance is the ability of a material to resist the crack propagation owing to complex stress profiles generated by the impact. In contrast, damage tolerance, whether based on the residual strength/impact energy or the residual strength/damage width relationship, is the ability of a material to tolerate the complete failure under monotonic loading. A better damage tolerance has been attributed to higher interlaminar fracture toughness, particularly in mode II shear,[29–31] and higher ductility and fracture toughness of the matrix material.[29,32] The better correlation of the residual compressive strength with the matrix ductility, particularly non-linear inelastic strains and mode II interlaminar fracture toughness, than with mode I interlaminar fracture toughness indicates that failure in CAI tests is essentially controlled more by the size of damage on impact than by subsequent resistance of the material to propagation of the damage.[5] It is normally assumed that the major damage modes are shear mode II delamination induced by bending, and opening mode I delamination followed by buckling, respectively, in the low-energy impact test and the subsequent compression-after-impact test.

Although it is still premature to say which of the surface treatment conditions offers the best combination of mechanical properties, the impact response of woven E-glass fabric composite laminates can be summarised in the following. The damage area and the corresponding residual compressive strength after impact increase with increasing impact energy. The damage area was larger on the back surface than on the front surface of impact, confirming the general trend of impact response. The total damage area measured on the back surface of the laminate, including that due to the fibre/matrix interface debonding, was highest in the order of the laminates containing 0·4 wt% γ-GPS, 0·01 wt% γ-MPS and other γ-MPS concentrations. Apart from the total damage area, the variations in the fibre/matrix interphase properties caused by different silane agents and concentration had marginal influence on other impact response parameters, including the major damage area and the residual compressive strength. The increase in silane concentration of γ-MPS slightly improved both the damage resistance and damage tolerance of the laminate in terms of the incipient impact energy, U_i, the threshold impact energy, U_0, and threshold damage width, c_0.

The impact test and the subsequent compression test successfully discriminated between materials, and are relevant to the assessment of damage induced as well as to the assessment of degradation in strength as a consequence of the damage. In particular, the compression test, which is chosen to evaluate the residual properties after impact, is proved to be useful as it induces failure owing to the cracks propagated from the existing damage. However, as both the incipient energy and the threshold energy are expected to be dependent on the loading geometry and dimensions of the structure,[33] these impact parameters are not material constants, but can only be used for comparison purposes.

ACKNOWLEDGEMENTS

The authors are most grateful to Nitto Boseki Co., Japan, for supplying the woven glass fabrics. JKK would like to acknowledge the continuing support of the project from the Research Grants Council (RGC) of Hong Kong. YH was on study leave from the Faculty of Textile Science, Kyoto Institute of Technology, Kyoto, Japan, to the Hong Kong University of Science and Technology, Hong Kong when this work was performed. Part of the paper has been presented at the 5th Symposium on Interfacial Science on Composite Materials (SIMS-V), which was held in May 1996 in Fukuoka, Japan.

REFERENCES

1. Cantwell, W. J. and Morton, J., Impact resistance of composite materials—a review. *Composites*, 1991, **22**, 347–362.
2. Roger, K. F., Sidey, G. R. and Kinston-Lee, D. M., Ballistic impact resistance of carbon-fibre laminates. *Composites*, 1971, **2**, 237–241.

3. McGarry, F. J., Mandell, J. F. and Kawamoto, J., Impact resistance of rubber modified carbon fibre composite. In *Proc. 21st Int. SAMPE Conf. on Advanced Composites*. Society for the Advancement of Materials and Process Engineering, Covina, California, 1989, pp. 195–205.
4. Williams, J. G. and Rhodes, M. D., Effect of resin on impact damage tolerance of graphite/epoxy laminates. In *Composite Materials: Testing and Design (Sixth Conf.)*, ASTM STP 787, ed. I. M. Daniel. American Society for Testing and Materials, Philadelphia, Pennsylvania, 1982, pp. 450–480.
5. Kim, J. K., Mackay, D. B. and Mai, Y. W., Drop-weight impact damage tolerance of CFRP with rubber modified epoxy matrix. *Composites*, 1993, **24**, 458–494.
6. Kim, J. K. and Mai, Y. W., Interfaces in composite. In *Structure and Properties of Fiber Composites*, Materials Science and Technology Series Vol. 13, volume editor T. W. Chou. VCH Publishers, Weinheim, Germany, 1993, Ch. 6, pp. 239–289.
7. Ishida, H., A review of recent progress in the studies of molecular and microstructure of coupling agents and their functions in composites, coating and adhesive joints. *Polym. Compos.*, 1984, **5**, 101–123.
8. Cheng, T. H., Jones, F. R. and Wang, D., Effect of fibre conditioning on the interfacial shear strength of glass fibre composites. *Compos. Sci. Technol.*, 1993, **48**, 89–96.
9. Koenig, J. L. and Emadipour, H., Mechanical characterisation of the interfacial strength of glass reinforced composites. *Polym. Compos.*, 1985, **6**, 142–150.
10. Suzuki, Y., Maekawa, Z., Hamada, H., Yokoyama, A., Sugihara, T. and Hojo, M., Influence of silane coupling agents on interlaminar fracture in glass fibre fabric reinforced unsaturated polyester laminates. *J. Mater. Sci.*, 1993, **28**, 1725–1732.
11. Hamada, H., Kotaki, M. and Hirai, Y., Effect of surface treatment and weave structure on mode I interlaminar fracture behaviour of glass woven fabric composites. In *Proc. 10th Int. Conf. on Composite Materials (ICCM-10)*, Whistler, Canada. Woodhead Pub. Ltd, Cambridge, UK, 1995, pp. 643–650.
12. Bequignat, R., Krawczak, P., Cantwell, W., Schramuzzino, P., Desaeger, M., Verpoest, I., Hamada, H., Hirai, Y., Kotaki, M., Hojo, M., Kim, J. K., Kocsis, J. K., Mackin, T. J., Mayer, J., Morii, T. and Tanimoto, T., Influence of different glass fibre sizings on the mechanical properties of glass fabric composites: report on a round robin test. In *Proc. 10th Int. Conf. on Composite Materials (ICCM-10)*, Whistler, Canada. Woodhead Pub. Ltd, Cambridge, UK, 1995, pp. 597–603.
13. Hirai, Y., Hamada, H. and Kim, J. K., Effect of silane coupling agents on impact performance of glass woven fabric laminates. In *Proc. 5th Symp. of Interfacial Materials Science on Composites (SIMS-V)*, Fukuoka, Japan, May 1996, pp. 160–163.
14. Kim, J. K., Leung, L. M., Lee, R. S. W. and Hirai, Y., Impact performance of a woven fabric CFRP laminate. *Polym. Polym. Compos.*, 1996, **4**, 549–561.
15. Cairns, D. S. and Lagace, P. A., A consistent engineering methodology for the treatment of impact in composite materials. *J. Reinf. Plast. Compos.*, 1992, **11**, 395–412.
16. Ghasemi-Nejhad, M. N. and Parvizi-Majidi, A., Impact behaviour and damage tolerance of woven carbon fibre-reinforced thermoplastic composites. *Composites*, 1990, **21**, 155–168.
17. Caprino, G., Residual strength prediction on impacted CFRP laminates. *J. Compos. Mater.*, 1984, **18**, 508–518.
18. Wardle, M. W. and Zahr, G. E., Instrumented impact testing of aramid-reinforced composite materials. In *Instrumented Impact Testing of Plastics and Composite Materials*, ASTM STP 936, ed. S. L. Kessler, G. C. Adams, S. B. Driscoll and D. R. Ireland. American Society for Testing and Materials, Philadelphia, Pennsylvania, 1987, pp. 219–235.
19. Hirai, Y., Hamada, H. and Kim, J. K., Damage modes in impact loading of glass woven fabric composites. *Adv. Compos. Lett.*, 1996, **5**, 56–60.
20. Choi, H. Y., Downs, R. J. and Chang, F. K., A new approach toward understanding damage mechanisms and mechanics of laminated composites due to low-velocity impact: part I—experiments. *J. Compos. Mater.*, 1991, **25**, 992–1011.
21. Lee, S. M. and Zahuta, P., Instrumented impact and static indentation of composites. *J. Compos. Mater.*, 1991, **25**, 204–222.
22. Poon, C., Benak, T. and Gould, R., Assessment of impact damage in toughened resin composites. *Theor. Appl. Fract. Mech.*, 1990, **13**, 81–97.
23. Caprino, G., On the prediction of residual strength for notched laminates. *J. Mater. Sci.*, 1983, **18**, 2269–2273.
24. Preuss, T. E. and Clark, G., Use of time-of-flight C-scanning for assessment of impact damage in composites. *Composites*, 1988, **19**, 145–148.
25. Babic, L., Dunn, C. and Hogg, P. J., Damage development and its significance in GRP subjected to impact. *Plast. Rubb. Process. Applic.*, 1989, **12**, 199–207.
26. Prichard, J. C. and Hogg, P. J., The role of impact damage in post-impact compression testing. *Composites*, 1990, **21**, 503–511.
27. Lankford, J., Compressive failure of fibre reinforced composite buckling, kinking and the role of the interphase. *J. Mater. Sci.*, 1995, **30**, 4343–4348.
28. Dorey, G., Damage tolerance and damage assessment in advanced composites. In *Advanced Composites*, ed. I. K. Partridge. Elsevier Applied Science, London, 1989, Ch. 11.
29. Evans, R. E. and Master, J. E., A new generation of epoxy composites for primary structural applications: materials and mechanics. In *Toughened Composites*, ASTM STP 937, ed. H. J. Johnston. American Society for Testing and Materials, Philadelphia, Pennsylvania, 1987, pp. 413–436.
30. Recker, H. G., Altstadt, V., Eberle, W., Folda, T., Gerth, D., Heckmann, W., Ittemann, P., Tesch, H. and Weber, T., Toughened thermosets for damage tolerance carbon fibre reinforced composites. *SAMPE J.*, 1990, **26**, 73–78.
31. Bradley, W. L., The effect of resin toughness on delamination toughness and post impact compression strength. In *Proc. 'Benibana' Int. Symp. on How to Improve the Toughness of Polymers and Composites—Toughness, Fracture and Fatigue of Polymers and Composites*, Yamagata, Japan, 1990, pp. 221–230.
32. Hirschbuehler, K. R., A comparison of several mechanical tests used to evaluate the toughness of composites. In *Toughened Composites*, ASTM STP 937, ed. H. J. Johnston. American Society for Testing and Materials, Philadelphia, Pennsylvania, 1987, pp. 61–73.
33. Zhou, G., Prediction of impact damage thresholds of glass fibre reinforced laminates. *Compos. Struct.*, 1995, **31**, 185–193.